GEOPHYSICS, VOL. 81, NO. 5 (SEPTEMBER-OCTOBER 2016); P. E279–E285, 10 FIGS.
10.1190/GEO2014-0564.1

Opposing-coils transient electromagnetic method focused near-surface resolution

Zhenzhu Xi[1], Xia Long[2], Long Huang[2], Sheng Zhou[2], Gang Song[3], Haitao Hou[2], Xingpeng Chen[3], Liang Wang[3], Wei Xiao[3], and Qingxing Qi[3]

ABSTRACT

The transient electromagnetic (TEM) method is a commonly used, nonintrusive, geophysical method, but inherent mutual induction between the transmitter (TX) and receiver (RX) coils strongly influences the measurements. We have developed an opposing-coils configuration to greatly reduce this effect. Three coils are used in this system. The upper opposing coil is physically the same as the lower TX coil, and they are concentric and parallel to the middle RX coil. A pair of currents with equal amplitudes but reverse directions is injected into the opposing and TX coils. Theoretical calculations in free space show that the received magnetic field by the RX coil is zero, which indicates that the mutual induction effect could be largely reduced. Physical experiments prove that an almost-pure secondary field could be acquired using this system. We have studied an optimal separation between the TX and opposing coils to guarantee that the primary magnetic field is powerful and the instrument is compacted for field work. Then, the efficient exploration depth of this system for typical geoelectric models was simulated to be approximately 15–50 m. Comparisons of simulated responses over highly conductive thick plates in free space and a field test over a culvert structure between this system and EM-47 showed that the system has enhanced sensitivity and lateral resolution. This system can be used in near-surface investigations, e.g., groundwater, environmental, and engineering investigations.

INTRODUCTION

The transient electromagnetic (TEM) method is a commonly used, nonintrusive, geophysical method of measuring the secondary electromagnetic field induced by transient pulse sources. It has been widely used to map geologic structure in search of mineral deposits, oil and gas, groundwater, and geothermal sources. It is also the preferred method for locating subsurface metal objects, such as abandoned wells, pipelines, and unexploded ordnance (Asten and Andrew, 2012; Swidinsky et al., 2012; Abu Rajab and El-Naqa, 2013; Frenkel and Yakovlev, 2013; Kukita and Mizunaga, 2013).

The TEM technique measures the secondary electromagnetic field excited by underground anomalies after switching off the imposed current in the TX coil. Ideally speaking, with a zero switch-off time, the secondary electromagnetic field can carry the conductivity information of the subsurface in full scale. However, because of the inherent mutual induction between the TX and RX coils, the switch-off time hardly approaches zero. Thus, the measured field always contains the secondary and the primary fields. The mutual induction becomes stronger when the TX coil becomes smaller and closer to the RX coil. Particularly, this mutual induction strongly influences the near-surface TEM systems recently developed, which use small TX coils to effectively resolve near-surface explorations. In addition, the secondary electromagnetic field at the RX coil may be several orders of magnitude smaller than the primary field (Telford et al., 1990), and separation of the measured total electromagnetic field into its primary and secondary parts is difficult

Manuscript received by the Editor 1 December 2014; revised manuscript received 15 January 2016; published online 7 July 2016.
[1]Central South University, School of Geosciences and Info-Physics, Changsha, Hunan Province, China. E-mail: xizhenzhu@163.com.
[2]Central South University, School of Geosciences and Info-Physics, Changsha, Hunan Province, China and Hunan 5D Geosciences Co. Ltd., Changsha, Hunan Province, China. E-mail: longxia001-ren@163.com; 363048765@qq.com; zhousheng.11@163.com.
[3]Hunan 5D Geosciences Co. Ltd., Changsha, Hunan Province, China. E-mail: 22557899@qq.com.

(Nabighian and Macnae, 1991). The mixture of the primary field with the secondary field at an early period leads to a blind region in the shallow surface in TEM exploration.

To efficiently narrow the blind region, Louise et al. (1995) and Zonge International Inc. (2015) try to shorten the switch-off time by reducing the size of the TX coil. However, as discussed above, the smaller TX coil is strongly influenced by the mutual induction. Smith and Balch (2000) and Walker and Rudd (2009) propose calculating the theoretical primary field caused by the mutual induction and then subtract it from the measured inductive response. However, due to the complexity of the underground structures, there is always a discrepancy between the theoretical calculation and actual measurement. Kuzmin and Morrison (2011) try to use a bucking coil positioned in a substantially concentric and coplanar orientation relative to the TX and the RX coils. Then, by adjusting the coil size and coil turn, the primary field measured by the RX coil could be approximately zero. This design effectively minimizes the mutual induction between the TX and RX coils, and is frequently used in the towed TEM system. However, this instrument requires a large operation space, which is not available in some areas, such as in advanced tunnel exploration, urban underground pipeline detection, and so on.

The opposing-coils TEM system is different from the device proposed by Kuzmin and Morrison (2011). We applied two current coils (shown in Figure 1), the lower as the TX coil, and the upper as the opposing coil, which was positioned concentric and parallel to the RX and TX coils. The RX coil is equidistant to the TX and opposing coils. A pair of currents with equal value but reverse directions is injected to the TX and opposing coils. In terms of this special arrangement, the primary field received at the RX coil is zero, which means that the mutual induction effect is efficiently eliminated. It is quite suitable for a small TX coil TEM system aiming at shallow subsurface detection.

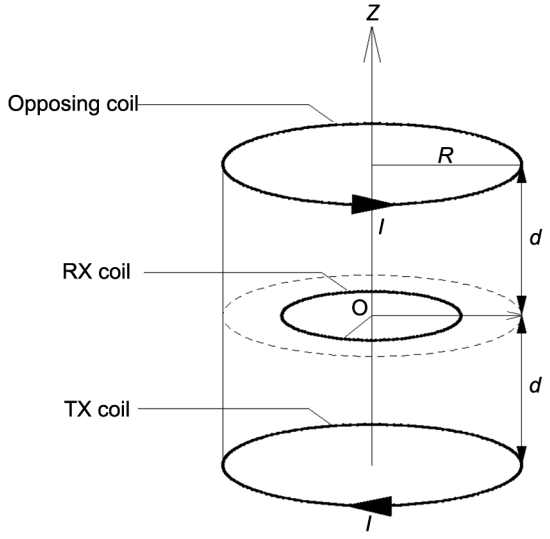

Figure 1. The geometric configuration of the opposing-coils TEM system. Two current coils are adopted. The lower is the TX coil, and the upper is the opposing coil. The RX coil is in the middle of the two current coils. The three coils are parallel and concentric to each other. The distance between the RX coil, the opposing coil, and the TX coil is denoted by the symbol d. The currents (with amplitude of I) in the opposing coil and TX coil are equal and reverse in their direction.

We began studying opposing-coils TEM since 2012, and we developed a prototype in 2013. Meanwhile, Allen (2013) introduces a preliminary idea about using the opposing coil for the towed TEM survey.

In this work, the opposing-coils TEM system was analyzed, designed, developed, and tested. We first developed the basic theory of the opposing-coils TEM and its performance to eliminate the mutual induction effect. Then, we studied the influence of the distance between the two opposing coils onto the primary field. In addition, we estimated the possible exploration depth. Finally, a simple model simulation and a corresponding field test were performed to qualitatively demonstrate that this technique has enhanced sensitivity and lateral resolution.

Background theory

The expressions for the magnetic field of a single coil with radius R, carried current I, and centered at the origin in the spherical coordinates system in free space is derived by Jackson (1998). Through coordinate transformation, the expressions in the cylindrical coordinate are expressed as

$$B_r = \frac{\mu_0 I z k}{8\pi r\sqrt{rR}}\left[-2K(k) + \frac{2-k^2}{1-k^2}E(k)\right], \tag{1}$$

$$B_z = \frac{\mu_0 I k}{8\pi\sqrt{rR}}\left[2K(k) + \frac{Rk^2 - (2-k^2)r}{r(1-k^2)}E(k)\right], \tag{2}$$

$$B_\theta = 0, \tag{3}$$

where μ_0 is the magnetic permeability in free space, r is the radial distance of the observation point, z is the vertical coordinate, $k = \sqrt{4Rr/[z^2 + (R+r)^2]}$, and $K(k)$ and $E(k)$ are the first and second kind of complete elliptic integral, respectively,

$$K(k) = \int_0^{\frac{\pi}{2}} \frac{d\theta}{\sqrt{1 - k^2\sin^2\theta}}, \tag{4}$$

$$E(k) = \int_0^{\frac{\pi}{2}} \sqrt{1 - k^2\sin^2\theta}\, d\theta. \tag{5}$$

Based on the above formulas, the total magnetic field can be computed using field superposition of the opposing coil and TX coil.

Primary magnetic field vectors of the opposing-coils TEM system

The opposing-coils TEM system, as a new geophysical technique, measures a pure secondary electromagnetic field. It is necessary to explain the physical phenomenology behind this new configuration. To focus on understanding the physical basis, the free-space model was used to explore how this system eliminates the mutual induction effect between the TX and RX coils.

Using equations 1–3, the magnetic field of the opposing-coils TEM system is calculated. In the calculation, R is 0.6 m, d is 0.2 m, z equals −0.2 m for TX coil, and z equals 0.2 m for the opposing coil. The magnetic field vectors on the central cross plane are illustrated in Figure 2. We observe that on the $z = 0$ plane where the RX coil is located, the vectors are horizontal, which means there is no vertical magnetic field component, and only the horizontal magnetic field component exists. Therefore, the primary magnetic field flux through the RX coil is zero. It will never cause primary induction voltage in the RX coil when currents in the TX and opposing coils are turned off simultaneously. So, the mutual induction effect in the conventional TEM method can be eliminated. The key idea of success is to guarantee that the currents in the opposing coil and TX coil are equal with reverse directions and delay simultaneously. This is easy to realize by connecting the two coils in series.

Influence of RX coil location on measured TEM signals

The free-space simulations show that on the center plane of the opposing-coils TEM system, the RX coil could pick up a pure secondary magnetic field. But any alignment error will introduce primary field into the RX coil. In this section, a physical test was used to analyze the variation of the measured field when alignment error exists.

Based on the previous discussion, a preliminary prototype as shown in Figure 3 has been constructed to carry out the test. The opposing coil and TX coil are 1.2 m in diameter and 10 turns. Distance between the opposing coil and TX coil is 0.3 m. The RX coil is 0.5 m in diameter and 100 turns with effective area of 19.63 m^2. In this paper, the physical test was carried out in Lugu Park of Changsha, Hunan Province, China. In the test, the transmitting frequency is 25 Hz, and transmitting current is 8 A.

In the test, we fixed the distance between the opposing coil and TX coil to 30 cm, i.e., TX coil at $z = -15$ cm, and the opposing coil at $z = 15$ cm. The RX coil was moved from b1 to b2, b3 (the prefix b represent below $z = 0$ plane), and to o-plane (almost at $z = 0$), then to a1, a2, and a3 (the prefix a represent above $z = 0$ plane). The measured induced voltage ε is shown in Figure 4.

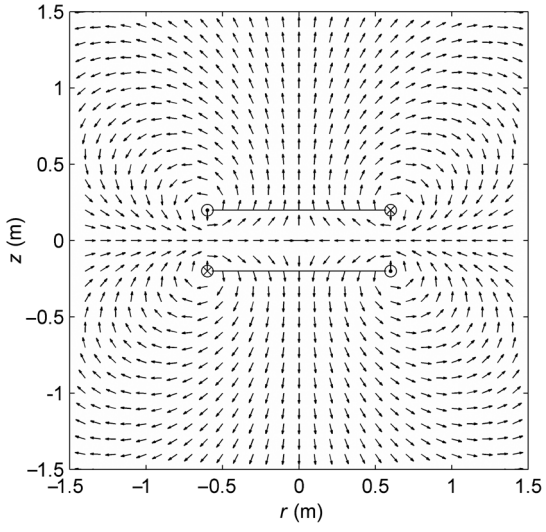

Figure 2. The magnetic field vector direction on the central cross section of the model given in Figure 1. Here, R is 0.6 m and d is 0.2 m. The lower line represents the TX coil, and the upper line represents the opposing coil. On the center plane of $z = 0$, there is no vertical component of the magnetic field. Only the horizontal component of the magnetic field exists.

Results show that when the RX coil was moved close to the $z = 0$ plane, the induced voltage decreased. When the RX coil is on the b1 ($z = -1.2$ cm) plane, it is more than 100 times larger than that when the RX coil is on the o-plane ($z \approx 0$). When the RX coil passed the $z = 0$ plane, the induced voltage in early times turned to be negative, and the value increased when the RX coil was moved away from the $z = 0$ plane. It was shown that the RX coil location has a serious influence on the induced voltage, and the influence lasts up to approximately 90 μs. After that time, all the ε-t curves tend to be the same, which means that the RX coil location has little influence on the induced voltage.

It is analyzed as follows. The induced voltage ε is the vector superposition of three parts: primary induced voltage ε_1, secondary induced voltage ε_2, and EM noise. If the EM noise is much smaller than the secondary induced voltage, ε approximately equals the sum of ε_1 and ε_2. When the opposing coil and TX coil are fixed and stationary, ε_2 will stay approximately the same. When the RX coil is correctly located on the $z = 0$ plane, $|\varepsilon_1|$ is equal to 0. The further it is away, the larger $|\varepsilon_1|$ will be. In the earlier period, $|\varepsilon_1|$ is far larger than $|\varepsilon_1|$. So, ε changes with the RX coil location. When the RX coil passes $z = 0$ plane, sign of ε_1 flips, so does the sign of ε. The $|\varepsilon_1|$ decays with time, and after approximately 90 μs, $|\varepsilon_1|$ is much smaller than $|\varepsilon_1|$, so ε approximately equals ε_2. That is why all the ε-t curves tend to be the same after approximately 90 μs.

Influence of distance between the TX and opposing coils on TEM primary and secondary field

The reliability of any electromagnetic method is governed by the signal-to-noise ratio (S/N) at the receiver (Szarka, 1988). The strength of the primary field plays an important role on S/N. Because of the introduction of the opposing coil, whose electromagnetic field cancels out the primary field of the TX coil, the strength of primary field should be considered. To enhance the primary field, we can increase the radius of the TX coil, the turn of wire, and the amplitudes of currents. However, in the field, radius and turns of the TX coil have been predetermined and can hardly be changed. Then, a possible solution is to increase the amplitudes of currents. Due to the opposing coil, the distance between the opposing coil and the TX coil is another factor.

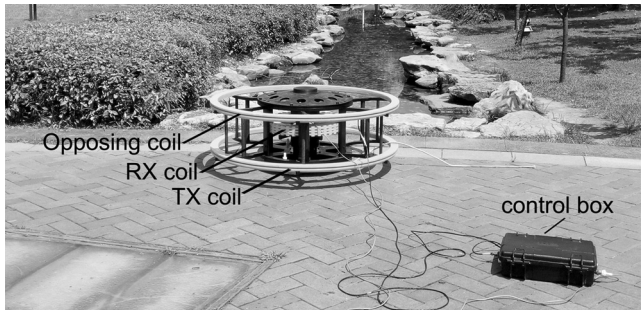

Figure 3. The opposing-coils TEM prototype. The opposing coil and TX coil are 1.2 m in diameter and 10 turns. Distance between the opposing coil and TX coil is 0.3 m. The RX coil is 0.5 m in diameter and 100 turns with an effective area of 19.63 m^2.

As shown in Figure 1, the TX coil is on the ground, the RX coil is on the $z = 0$ plane. We computed the primary vertical magnetic intensity (Bz) along the z-axis below $z = 0$ plane, with distance $2d$ equaling 20, 30, or 40 cm. The TX current is 10 A, the turn number is 10, and the TX coil radius is 0.6 m. The results are shown in Figure 5a. Here, Bz increases as d increases, as does the secondary induced voltage (Figure 5b). However, when d becomes larger, the system will be heavier, and the distance from the RX coil to the subsurface target will be larger, which in turn decreases the strength of the measured secondary field. Therefore, an optimal value of d should be determined. To reduce the size of the antenna, taking into account of the strength of the primary field, we recommend $2d$ as 30 cm.

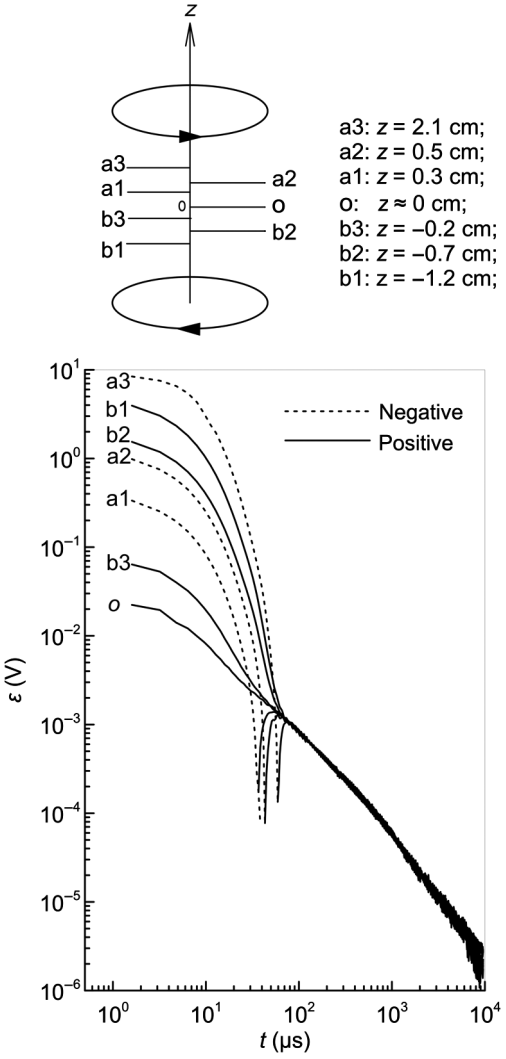

Figure 4. Influence of the RX coil location on measured TEM signals. The induced voltage was measured with the RX coil moving along the z-axis from b1 to b2, b3 (the prefix b represent below $z = 0$ plane), and to o-plane (almost at $z = 0$), then to a1, a2, and a3 (the prefix a represent above $z = 0$ plane). When RX coil moves close to $z = 0$, the induced voltage decreases. When the RX coil is on the b1 ($z = -1.2$ cm) plane, it is more than 100 times larger than when the RX coil is on the o-plane. When the RX coil moves across the $z = 0$ plane, the induced voltages in early times turn out to be negative, and the values increase when the RX coil moves away from $z = 0$ plane.

Investigation depth of the opposing-coils TEM system

Investigation depth is a key parameter for an exploration method. It can be used to guide the field work, e.g., application areas. In this section, we used the algorithm proposed by Zonge Engineering and Research Organization Inc. (1992) to estimate the exploration depth of the opposing-coils TEM system in a homogeneous half-space with resistivity of $1-1000$ Ωm.

In these calculations, the diameter of the opposing coils is 1.2 m, the turn number of wires is 10, the injected current is 10 A, the distance between the opposing coil and the TX coil is 0.3 m, the

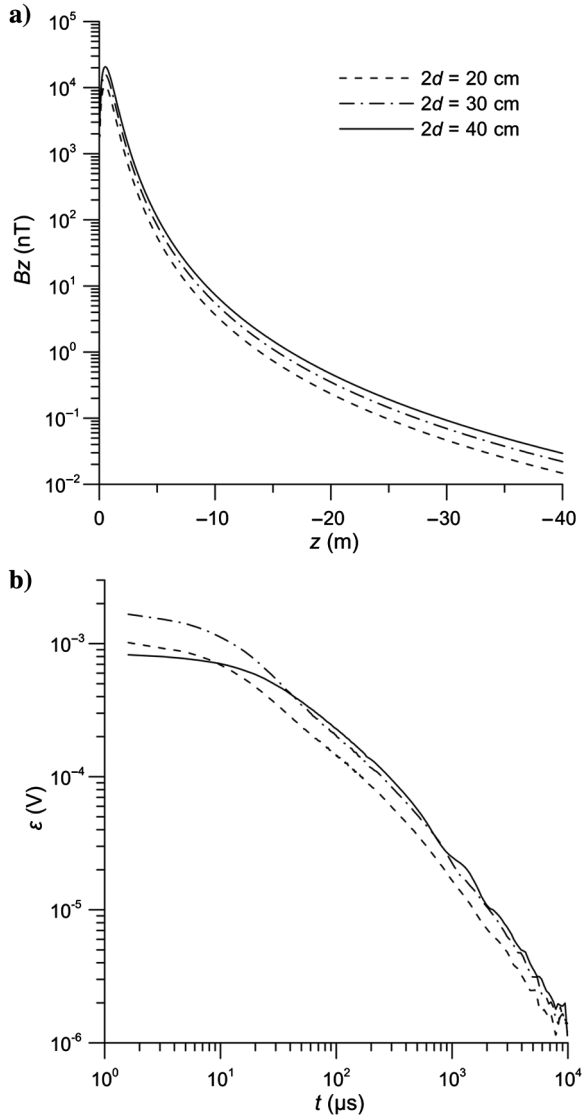

Figure 5. Influence of the distance between the TX coil and the opposing coil on the TEM primary and secondary field. (a) The primary vertical magnetic field along the z-axis below the $z = 0$ plane, for cases of different distances between the TX coil and the opposing coil. (b) Measured induced voltage for cases of different distances between the TX coil and the opposing coil.

diameter of the receiving coil is 0.5 m, and the turn number of the RX coil is 100, so the effective area of the RX coil is 19.63 m^2. The EM noise is supposed as 1 nV/m^2.

The secondary TEM response of the opposing-coils TEM system was computed by the superposition of the responses of the TX coil and the opposing coil, using Beowulf (Version 1.0. 3, 7 November 2007) supplied by AMIRA International (2008). The time t (in ms) was read from the decay curves when the induced voltage is equal to the EM noise.

According to Spies (1989), the diffusion depth was estimated by the formula

$$\delta_{TD} = \sqrt{2\rho t/\mu_0}. \quad (6)$$

Figure 6 shows the investigation depth in a nomograph for a typical background EM noise level of 1 nV/m^2. When the half-space resistivity ρ equals 1 Ωm, the diffusion depth δ_{TD} equals 16.8 m; when ρ is 10 Ωm, δ_{TD} is 25.5 m; when ρ becomes 100 Ωm, δ_{TD} is 35.4 m; and when ρ becomes 1000 Ωm, δ_{TD} is 50.1 m. These results indicate that the opposing-coils TEM system is suitable for near-surface exploration.

Numerical and field tests using opposing-coils TEM and EM47 configurations

The above analysis proved that the opposing-coils TEM method could obtain pure secondary field, which makes it applicable in near-surface investigations. To further qualitatively demonstrate the enhanced sensitivity and lateral resolution of this system, in this section a numerical model and field test were used. In addition, the results of this system and the Geonics EM47 system were compared.

First, the numerical model of highly conductive thick plates was used. The responses were calculated using MAXWELL software (version 5.9.1) supported by EMIT (2013) for the opposing-coils TEM system and conventional single central loop. The model and calculation results are shown in Figure 7. It is a simple model of four highly conductive thick plates (conductivity is 1000 S/m, thickness is 2 m, strike length is 10 m, and depth extent is 10 m) in a half-space of 0 S/m, with 2 m separation between each other, and 4 m below the surface. Because of the limitation of the MAXWELL software, 10 turn 1.2 × 1.2 m square coil configuration was used for the opposing-coils TEM system. The 1 turn 5 × 5 m central loop configuration was used for the conventional single central loop. In other words, the effective receiving area is 20 m^2 and transmitting current is 10 A for both systems. The simulated TEM responses are shown in Figure 7. The responses of the 1.2 × 1.2 m opposing-coils configuration are smaller, but there are four peak responses corresponding to the center top of the plates, which means it distinguishes the four thick plates very well. The response of 5 × 5 m loop shows a total TEM response of the four thick plates in a larger amplitude, which is not able to clearly identify the four thick plates. It indicates that the opposing-coils TEM system has advantages in lateral resolution to detect shallow small target bodies.

Correspondingly, a field test was taken over a dam drainage culvert near Xiangjiang River in Changsha City, Hunan Province. In June 2015, we conducted an investigation test using the opposing-coils TEM prototype and EM47 for comparison. We deployed one profile across the drainage culvert. Measurement array locations were sketched in Figure 8. A, B, C, D, E, F, J, K, and L in the figure indicate sites on the load-bearing walls of steel bars. Right above the drainage culvert (profile 50–80 m), station spacing is 0.5 m, and on two sides of the drainage culvert (profiles 5–50 and 80–125 m), site separation is 2 m. The 10 turn 1.2 m diameter circular coils with

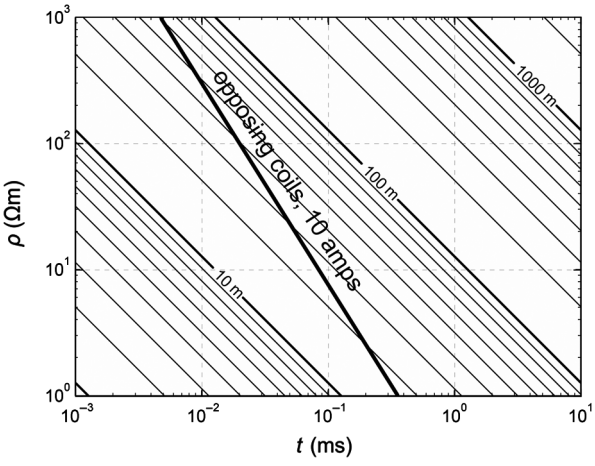

Figure 6. Investigation depth of our opposing-coils TEM prototype with a noise level of 1 nV/m^2.

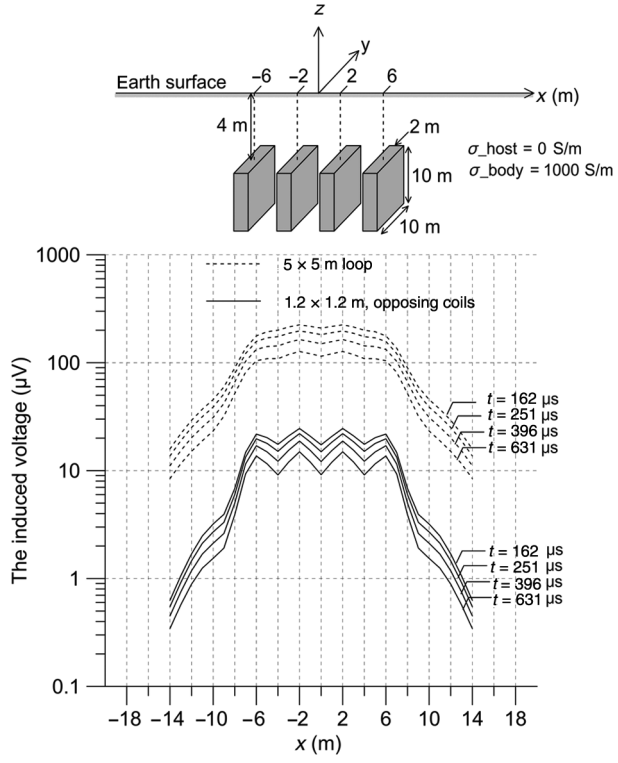

Figure 7. Simplified model calculation by Maxwell software. Four identical 1000 S/m conductive thick plates (2 × 10 × 10 m) are located in a 0 S/m half-space 4 m below the earth's surface. The separation among the four plates is 4 m. The responses of 1.2 × 1.2 m opposing-coils configuration are smaller, but there are four peak responses corresponding to the center top of the plates. Although the responses of 5 × 5 m loop show a total TEM response of the four thick-plates in larger amplitude, which are not able to well distinguish the four thick plates.

8.6 A current were used as the TX and opposing coils for the opposing coils-TEM prototype. For EM47, a single turn 5×5 m TX loop was applied with receiving antenna in the center, and the TX current is 2.36 A.

Measured data by EM47 are shown in Figure 9. Right over the drainage culvert (profile 50–80 m), there is an obviously high-value anomaly from 27 to 6978 μs, which is represented as a total TEM response of the steel culvert structure. Measured data by the opposing-coils TEM prototype (Figure 10) show a relatively high-value anomaly from 3.2 to 9844.8 μs in the same section, with magnitude lower than that measured by EM47. This lower magnitude is caused by the opposing coil, which cancels out some primary field. However, this method picked up anomalous peaks at A, B, C, D, E, F, G, H, I, J, and K sites. According to the model simulation in Figure 7, they can be considered as responses of the steel culvert structures.

On two sides of the drainage culvert (profiles 5–50 and 80–125 m), measured data by the two systems are lower, seen as background responses. There are disorders for data measured by EM47, which could be influence of urban cultural noise. Although there is a relatively good continuity for data measured by the opposing-coils TEM prototype, which indicates that the opposing-coils TEM has the advantage of suppressing noise to get high-quality, stable, and reliable signal data. In addition, with careful observation, there are anomalies presenting at 26, 34, 92, 104, and 118 m for data measured by the opposing-coils TEM prototype, which also presents in different degrees for data measured by EM47, and are caused by an unknown anomalous body underground.

Figure 8. Illustration of the field test. Symbols A, B, C, D, E, F, J, K, and L in the figure indicate different sites on the load-bearing walls of steel bars. Right above the drainage culvert (profiles 50–80 m), site separation is 0.5 m, and on two sides of the drainage culvert (profiles 5–50 and 80–125 m), the site separation is 2 m.

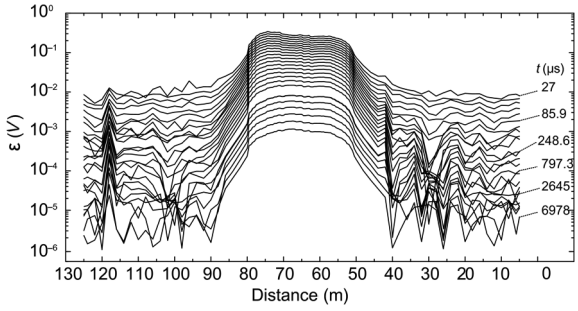

Figure 9. Measured induced voltage profile by the Geonics EM-47 system. A single-turn 5×5 m TX loop was applied with an RX antenna in the center; the TX current is 2.36 A. The curves showed the total TEM response of the steel culvert structures.

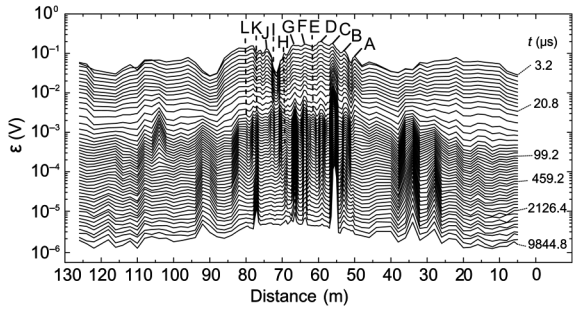

Figure 10. Measured induced voltage profile by our opposing-coils TEM prototype. The opposing coil and TX coil are 1.2 m in diameter and 10 turns with injected current of 8.6 A. Distance between the opposing coil and the TX coil is 0.3 m. The RX coil is 0.5 m in diameter and 100 turns with effective area of 19.63 m^2. Anomalous peaks in sites A–K reflect the steel culvert structure shown in Figure 8.

CONCLUSIONS

The opposing-coils TEM configuration was presented. Theoretical calculations and physical experiments prove that it is feasible to eliminate the mutual induction effect between the TX and the RX coils and obtain almost pure secondary electromagnetic field. The field strength increases as the distance between the opposing and TX coils increases. To reduce the configuration size, the distance $2d$ is recommended as 30 cm. For the opposing-coils TEM prototype with 10 A current in condition of 1 nV/m^2 noise level, the numerically calculated maximum exploration depth was 16.8–51.6 m in 1–1000 Ωm case. The numerical simulations of four high conducting thick plates and field test over the dam drainage culvert along the Xiangjiang River using the opposing-coils TEM prototype and EM47 proved that the opposing-coils TEM method can be used for near-surface detection with enhanced sensitivity and lateral resolution. In addition, it is highly robust even with some background noise. This system can be adapted to the application of near-surface investigations.

ACKNOWLEDGMENTS

We wish to thank the colleague of our company for field work. Thanks are given to Z.-Y. Ren and W.-J. Feng for reading the early version of this manuscript.

REFERENCES

Abu Rajab, J. S., and A. R. El-Naqa, 2013, Mapping groundwater salinization using transient electromagnetic and direct current resistivity methods in Azraq Basin: Geophysics, **78**, no. 2, B89–B101, doi: 10.1190/geo2011-0362.1.

Allen, D., 2013, Towed transient electromagnetic survey using various loop configurations: 23rd Geophysical Conference, ASEG, Extended Abstracts, doi: 10.1071/ASEG2013ab020.

AMIRA International, 2008, P223-EM Modelling software, http://www.amirainternational.com/WEB/site.asp?section=news&page=projectpages/p223f_software, accessed 21 April 2016.

Asten, M. W., and C. Andrew, 2012, The quantitative advantages of using B-field sensors in time-domain EM measurement for mineral exploration and unexploded ordnance search: Geophysics, **77**, no. 4, WB137–WB148, doi: 10.1190/geo2011-0385.1.

EMIT, 2013, Electromagnetic imaging technology, Maxwell, http://www.electromag.com.au/Maxwell.php, accessed 21 April 2016.

Frenkel, M., and A. Yakovlev, 2013, Land hydrocarbon exploration using novel time-domain electromagnetic technology: 83rd Annual International Meeting, SEG, Expanded Abstracts, 780–784.

Jackson, J. D., 1998, Classical electrodynamics: Hamilton Printing Company, 180–182.

Kukita, S., and H. Mizunaga, 2013, UXO detection using small loop TEM method: Proceedings of the 11th SEGJ International Symposium, 94–97.
Kuzmin, P. V., and E. B. Morrison, 2011, Bucking coil and B-field measurement system and apparatus for time domain electromagnetic measurements: U.S. Patent 8,786,286.
Louise, P., V. F. Labson, M. C. Pfeifer, A. Becker, W. Frangos, G. M. Hoversten, M. Goldman, K. H. Lee, H. F. Morrison, H. D. M. Lean, D. D. Snyder, G. A. Newman, D. L. Alumbaugh, A. C. Tripp, M. S. Zhdan, S. H. Ward, D. V. Fitterman, T. P. Grover, and D. L. Wright, 1995, VETEM — A very early time electromagnetic system — The first year: Symposium on the Application of Geophysics to Engineering and Environmental Problems, 795–802.
Nabighian, M. N., and J. C. Macnae, 1991, Time domain electromagnetic prospecting methods: Electromagnetic Methods in Applied Geophysics, **2**, 427–520, doi: 10.1190/1.9781560802686.
Spies, B. R., 1989, Depth of investigation in electromagnetic sounding methods: Geophysics, **54**, 872–888, doi: 10.1190/1.1442716.
Smith, R. S., and S. J. Balch, 2000, Robust estimation of the band-limited inductive limit response from impulse-response TEM measurements taken during the transmitter switch-off and the transmitter off-time: Geophysics, **65**, 476–481, doi: 10.1190/1.1444741.
Swidinsky, A., S. Hölz, and M. Jegen, 2012, On mapping seafloor mineral deposits with central loop transient electromagnetics: Geophysics, **77**, no. 3, E171–E184, doi: 10.1190/geo2011-0242.1.
Szarka, L., 1988, Geophysical aspects of man-made electromagnetic noise in the earth — A review: Surveys in Geophysics, **9**, 287–318, doi: 10.1007/BF01901627.
Telford, W. M., L. P. Geldart, and R. E. Sheriff, 1990, Applied geophysics: Cambridge University Press.
Walker, S. E., and J. Rudd, 2009, Extracting more information from on-time data: 20th Geophysical Conference, ASEG, Extended Abstracts, 1–8.
Zonge Engineering and Research Organization Inc., 1992, Introduction to TEM. Extracted from practical geophysics II: Northwest Mining Association.
Zonge International Inc., 2015, NanoTEM® near-surface method, http://zonge.com/geophysical-methods/electrical-em/nanotem/, accessed 14 June 2015.